Available online at www.sciencedirect.com
ScienceDirect
International Journal of Refrigeration 30 (2007) 546–564
REVUE INTERNATIONALE DU FROID
INTERNATIONAL JOURNAL OF
refrigeration
www.elsevier.com/locate/ijrefrig

Decoupling features and virtual sensors for diagnosis of faults in vapor compression air conditioners

Haorong Li[a,*], James E. Braun[b]

[a]University of Nebraska-Lincoln, PKI-101 F, 1110 S, 67th street, Lincoln, NE 68182, USA
[b]Purdue University, West Lafayette, IN, USA

Received 13 October 2005; received in revised form 17 March 2006; accepted 7 July 2006
Available online 24 October 2006

Abstract

This paper describes the development and evaluation of features and virtual sensors that form the basis of a methodology for detecting and diagnosing multiple-simultaneous faults in vapor compression air conditioning equipment. The features were developed based upon a physical understanding of the system, cost considerations, and heuristics derived from experimental data and modeling results. Virtual sensors were developed in order to reduce the cost of implementation. The validity of the features and virtual sensors was evaluated using measurements from a variety of different air conditioners tested in a laboratory environment. More detailed evaluation results are presented in separate papers.

Keywords: Air conditioner; Refrigerated equipment; Process; Detection; Faults; Modelling

Dispositifs de découplage et capteurs virtuels utilisés pour diagnostiquer les anomalies dans les conditionneurs d'air à compression de vapeur

Mots clés : Conditionneur d'air ; Équipement frigorifique ; Procédé ; Détection ; Anomalies ; Modélisation

1. Introduction

Li and Braun [1] presented an overall methodology for detecting and diagnosing multiple-simultaneous faults in vapor compression air conditioners using low-cost measurements. The key to handling multiple faults lies in the identification of decoupling features which are uniquely dependent on individual faults. However, some decoupling features require expensive measurements. In this case, virtual sensors can be employed to reduce costs. Virtual sensors rely on low-cost measurements and models to estimate quantities necessary in determining decoupling features. The current paper describes the development and evaluation of features and virtual sensors utilized within the fault detection diagnostic (FDD) method presented by Li and Braun [1]. The resulting method uses the same measurements that have been proposed for FDD methods that only handle individual faults.

* Corresponding author. Tel.: +1 402 554 3271; fax: +1 402 554 2080.
E-mail address: haorongli@mail.unomaha.edu (H. Li).

0140-7007/$35.00 © 2006 Elsevier Ltd and IIR. All rights reserved.
doi:10.1016/j.ijrefrig.2006.07.024

Nomenclature

BF	Bypass factor
c_i	Correlation equation coefficients
$C_{p,air}$	Air specific heat
CompLeak	Compressor valve leakage
CondFoul	Condenser fouling
D	Discharge dew point temperature [°C]
$\Delta^2 P_{ll}$	Liquid-line filter/drier pressure difference residual [kPa]
ΔT_{ca}	Condenser air temperature difference [°C]
ΔT_{cond}	Condensing temperature residual [°C]
ΔT_{dis}	Discharge line temperature residual [°C]
ΔT_{ea}	Evaporator air temperature difference [°C]
ΔT_{ll}	Temperature difference across the liquid-line filter/drier [°C]
ΔT_{sc-sh}	Refrigerant charge diagnosis feature [°C]
$\Delta \dot{V}_{ca}$	Condenser air volume flow residual [$m^3\,s^{-1}$]
$\Delta \dot{V}_{ea}$	Evaporator air volume flow residual [$m^3\,s^{-1}$]
EvapFoul	Evaporator fouling
FDD	Fault detection and diagnosis
FXO	Fixed orifice
h_{dis}	Discharge line refrigerant enthalpy [$J\,kg^{-1}$]
h_{fg}	Vaporization enthalpy [$J\,kg^{-1}$]
h_{ll}	Liquid-line refrigerant enthalpy [$J\,kg^{-1}$]
h_{aie}	Evaporator inlet air enthalpy [$J\,kg^{-1}$]
h_{aoe}	Evaporator outlet air enthalpy [$J\,kg^{-1}$]
$h_{s,evap}$	Saturated air enthalpy at evaporator surface temperature ($T_{s,evap}$) [$J\,kg^{-1}$]
h_{suc}	Suction line refrigerant enthalpy [$J\,kg^{-1}$]
k_{sc}	Slope of refrigerant charge vs. liquid-line subcooling [$kg\,°C^{-1}$]
$k_{sc\|dc}$	Partial differential of subcooling to a certain driving condition [$kg\,°C^{-1}$]
k_{sh}	Slope of refrigerant charge vs. suction line superheat [$kg\,°C^{-1}$]
$k_{sh\|dc}$	Partial differential of superheat to a certain driving condition [$kg\,°C^{-1}$]
LLRestr	Liquid-line restriction
$\dot{m}_{ref}$	Refrigerant mass flow rate [$kg\,s^{-1}$]
$\dot{m}_{ref,esti}$	$\dot{m}_{ref}$ estimated by a virtual sensor [$kg\,s^{-1}$]
$\dot{m}_{ref,map}$	Refrigerant mass flow rate predicted using compressor map data [$kg\,s^{-1}$]
$\dot{m}_{ref,meas}$	$\dot{m}_{ref}$ measured by a real sensor [$kg\,s^{-1}$]
$\dot{m}_{ref,pred}$	$\dot{m}_{ref}$ predicted by a model [$kg\,s^{-1}$]
MAT	Mixed air temperature [°C]
N	Number of suction strokes per unit time
$p(\,)$	Refrigerant pressure function
$p_{sat}(\,)$	$p(\,)$ at saturated conditions
P_{down}	Orifice outlet pressure [kPa]
P_{ll}	Liquid-line pressure [kPa]
P_{ncg}	Non-condensable gas partial pressure [kPa]
$P_{ref,vapor}$	Refrigerant partial pressure [kPa]
P_{sat}	Saturated pressure [kPa]
P_{suc}	Suction pressure [kPa]
P_x	Expansion device upstream refrigerant pressure [kPa]
q_{loss}	Compressor heat loss [$J\,kg^{-1}$]
$\dot{Q}_{cap}$	Cooling capacity [$J\,s^{-1}$]
r_{ncg}	Mole ratio of non-condensable gas to total refrigerant
RefLeak	Refrigerant leakage
S	Suction dew point temperature
$t(\,)$	Refrigerant temperature function
$t_{sat}(\,)$	Refrigerant saturated temperature function
T_{aic}	Condenser inlet air temperature [°C]
T_{aie}	Evaporator inlet air temperature [°C]
T_{amb}	Compressor ambient air temperature [°C]
T_{aoc}	Condenser outlet air temperature [°C]
T_{aoe}	Evaporator outlet air temperature [°C]
T_{cond}	Condensing temperature [°C]
$T_{cond,meas}$	Measured condensing temperature [K]
$T_{cond,pred}$	Predicted condensing temperature [°C]
T_{dis}	Discharge line temperature [°C]
$T_{dis,meas}$	Measured discharge line temperature [°C]
$T_{dis,pred}$	Predicted discharge line temperature [°C]
T_{down}	Expansion device downstream temperature [°C]
T_{evap}	Evaporating temperature [°C]
T_{sat}	Saturated temperature [°C]
$T_{s,evap}$	Evaporator surface temperature [°C]
T_{sh}	Suction line superheat [°C]
$T_{sh,rated}$	T_{sh} at a rated condition [°C]
T_{sc}	Liquid-line subcooling [°C]
$T_{sc,rated}$	T_{sc} at a rated condition [°C]
T_{suc}	Suction line temperature [°C]
T_x	Expansion device upstream refrigerant pressure [°C]
TXV	Thermostatic expansion device
v_{ca}	Condenser air specific volume [$m^3\,kg^{-1}$]
v_{ea}	Evaporator air specific volume [$m^3\,kg^{-1}$]
v_{fg}	Specific volume change [$m^3\,kg^{-1}$]
v_{suc}	Suction line refrigerant specific volume [$m^3\,kg^{-1}$]
V	Displacement volume [m^3]
$\dot{V}_{ca}$	Condenser air volume flow rate [$m^3\,s^{-1}$]
$\dot{V}_{ca,pred}$	Predicted condenser air volume flow rate [$m^3\,s^{-1}$]
$\dot{V}_{ea}$	Evaporator air volume flow rate [$m^3\,s^{-1}$]
$\dot{V}_{ea,pred}$	Predicted evaporator air volume flow rate [$m^3\,s^{-1}$]
w_{pred}	Compressor specific work for normal operation [$m^3\,s^{-1}$]
w_{aie}	Evaporator inlet air humidity ratio [kg (kg dry air)$^{-1}$]
w_{aoe}	Evaporator outlet air (supply air) humidity ratio [kg (kg dry air)$^{-1}$]

$w_{s,evap}$	Saturated air humidity ratio at evaporator surface temperature [kg (kg dry air)$^{-1}$]
$\dot{W}$	Compressor power consumption [kW]
$\dot{W}_{map}$	$\dot{W}$, predicted by compressor map [kW]
$\dot{W}_{meas}$	$\dot{W}$, measured by a real sensor [kW]
$\dot{W}_{pred}$	$\dot{W}$, predicted by a model [kW]
X	Correlated variables

Greek letters

α_{loss}	Compressor heat loss ratio
η_v	Volumetric efficiency
χ_{ref}	Refrigerant quality
ϕ_{aie}	Evaporator inlet air relative humidity
ϕ_{aoe}	Evaporator outlet air relative humidity

Fig. 1 depicts the factors that affect the performance of a simple vapor compression system (steady-state driving conditions, faults, and dynamic disturbances) and state variables determined from measurements that have been previously proposed for fault detection and diagnostics. For a simple vapor compression system having fixed-speed fans and on/off control, the driving conditions that influence steady-state performance are the condenser inlet air temperature (T_{aic}) and the evaporator air temperature and relative humidity (T_{aie} and ϕ_{aie}). The FDD method considers the important and difficult to diagnose faults that impact system cooling capacity, efficiency and equipment life as documented by Breuker and Braun [2], including faults that degrade compressor flow capacity (e.g., compressor valve leakage), low or high refrigerant charge (leakage or inadequate charging during service), air-side fouling or loss of flow for the condenser or evaporator, a liquid-line restriction (e.g., filter/dryer clogging), and presence of a non-condensable gas. Dynamic disturbances include transients due to on/off cycling of the compressor or rapid changes in air inlet conditions due to a change in damper or control. A steady-state detector is typically employed to filter dynamic disturbances [3]. However, dynamics can sometimes provide additional features that can be used for FDD.

The state variables shown in Fig. 1 have been proposed by several investigators for FDD, including Rossi and Braun [4], Breuker and Braun [5], and Chen and Braun [6]. These variables are all expressed as temperatures or temperature differences, but may not all be measured directly. For instance, the evaporating and condensing temperatures (T_{evap} and T_{cond}) would often be determined from measurements of compressor suction and discharge pressure using saturation property relations. The superheat of the refrigerant leaving the evaporator (T_{sh}) is the difference between the suction line temperature and the saturation temperature at the suction line pressure. Similarly, subcooling of the refrigerant leaving the condenser (T_{sc}) is the difference between the saturation temperature at the condenser outlet pressure and the condenser outlet temperature. The condenser outlet pressure would often be estimated by assuming a negligible or small pressure drop across the condenser. The temperature differences across the liquid-line (ΔT_{ll}), evaporator air stream (ΔT_{ea}), and condenser air stream (ΔT_{ca}) are all determined from direct temperature measurements. The temperature of the compressor discharge gas (T_{dis}) is also measured directly. Any of the refrigerant temperature measurements would normally be determined from surface mounted sensors that are insulated.

The advantage of utilizing only temperatures as state variables is low cost. Ideally, all of the temperatures would be measured directly, eliminating the need for pressure sensors. This is the subject of ongoing research. Earlier FDD methods developed for vapor compression systems that utilize the state variables of Fig. 1, such as the statistical rule-based method of Rossi and Braun [4], are only applicable to diagnosing individual faults. Each of the states shown in Fig. 1 has some dependence on all of the faults. Therefore, in order to handle multiple-simultaneous faults, it is necessary to

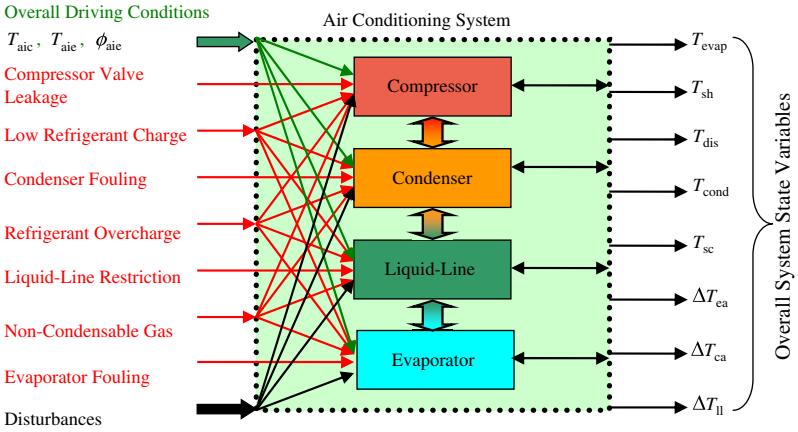

Fig. 1. State variable dependencies for vapor compression air conditioning equipment.

define alternative features that are uniquely dependent on individual faults. However, these decoupled features could be expensive to determine from direct measurements. Therefore, it is critical to incorporate virtual sensors in order to achieve practical FDD systems. Virtual sensors utilize models in order to estimate features from low-cost measurements. Ideally, the models should be simple and obtainable from information and data readily available from equipment manufacturers and should not require extensive training.

Fig. 2 depicts different models and their inputs and outputs for the FDD method of Li and Braun [1]. The inputs include both actual measurements (circled symbols) and variables determined from virtual sensors or simple combinations of actual measurements (bare symbols). The outputs are decoupled features (symbols within shaded ovals) and virtual sensor outputs needed by other modules. The actual measurements are the same as those used to determine the state variables in Fig. 1 and employed by previous FDD methods that only handle individual fault diagnoses. The following sections describe the development and evaluation of the features and virtual sensors for these modules. Unless otherwise noted, the features and virtual sensors rely on quasi-steady performance. Quasi-steady state is a condition where the state variables are close to their equilibrium values for a given set of external driving conditions. Several investigators [3,7] have developed steady-state detectors that could be utilized with this FDD method.

Data from a variety of sources [8–11] were utilized in the process of developing and evaluating decoupling features and virtual sensors. Breuker [8] collected two types of data under controlled conditions for a 3-ton rooftop air conditioner with a short-tube as the expansion device. One is normal operation data, including 135 sets over a wide range of driving conditions. The other is faulty operation data, including 120 sets for five kinds of faults with five load levels (20%, 40%, 60%, 80% and 100%) and five fault levels for each fault (only four fault levels for the evaporator fouling fault). Harms [9] collected experimental data under various refrigerant charge levels for a R22 system with thermostatic expansion valve as an expansion device. Shen [10] collected extensive experimental data under various charge levels for three R410a systems with both fixed orifice and

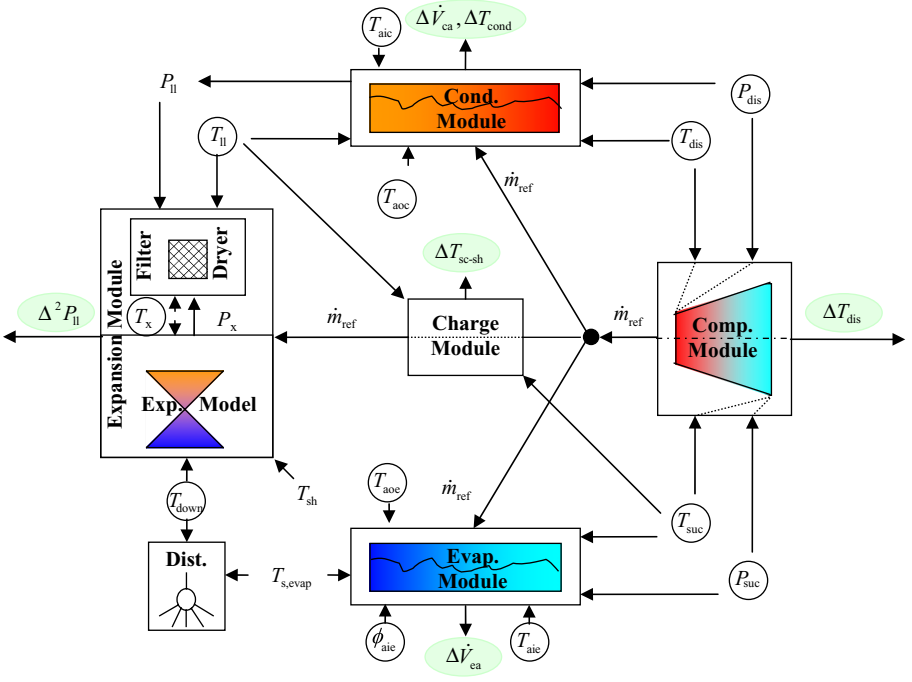

ΔT_{cond} - condenser temperature residual
$\dot{V}_{ca}$ - condenser volumetric air flow rate residual
$\dot{V}_{ea}$ - evaporator volumetric air flow rate residual
$\dot{m}_{ref}$ - refrigerant mass flow rate
P_{suc} - suction pressure
T_{aic} - condenser inlet air temperature
T_{aoc} - condenser outlet air temperature
T_{dis} - discharge temperature
T_{sh} - suction superheat

P_{dis} - discharge pressure
P_x - expansion device upstream pressure
T_{aie} - evaporator inlet air temperature
T_{aoe} - evaporator outlet air temperature
T_{down} - expansion device down stream pressure
T_{suc} - suction temperature

$\Delta T_{sc\text{-}sh}$ - charge level feature
ΔT_{dis} - discharge temperature residual
$\Delta^2 P_{ll}$ - liquid line pressure drop residual
P_{ll} - liquid line pressure
ϕ_{aie} - evaporator inlet air humidity
T_{ll} - liquid line temperature
T_x - expansion device upstream temperature

Fig. 2. FDD modules and their inputs and outputs.

thermostatic expansion valve as expansion devices. Li [13] collected additional transient data for developing liquid-line restriction decoupling feature.

2. Compressor module

2.1. Decoupling feature for compressor flow loss (valve leakage)

The steady-state performance of a compressor depends uniquely on suction pressure (P_{suc}), suction temperature (T_{suc}), and discharge pressure (P_{dis}). When a compressor develops leakage across a valve (suction or discharge) or an internal seal (e.g., piston-cylinder interface), then refrigerant mass flow rate decreases and compressor specific work increases compared to normal operation for a given condition. Both of these changes cause the discharge line temperature to increase significantly compared to normal operation. Under normal, steady-state operating conditions, the compressor discharge temperature can be predicted from

$$T_{dis,pred} = t\left(P_{dis}, h_{dis,pred}\right) \tag{1}$$

$$h_{dis,pred}(P_{suc}, T_{suc}, P_{dis}) = h_{suc}(P_{suc}, T_{suc}) + w_{pred}(P_{suc}, T_{suc}, P_{dis}) - q_{loss} \tag{2}$$

where

$$q_{loss} = \alpha_{loss} w_{pred}(P_{suc}, T_{suc}, P_{dis}) \tag{3}$$

$$w_{pred}(P_{suc}, T_{suc}, P_{dis}) = \frac{\dot{W}_{map}(P_{suc}, T_{suc}, P_{dis})}{\dot{m}_{ref,map}(P_{suc}, T_{suc}, P_{dis})} \tag{4}$$

where $t(\,)$ is the property function of the refrigerant, $h_{dis,pred}$ is the predicted discharge line refrigerant enthalpy, $T_{dis,pred}$ is predicted discharge line temperature, h_{suc} is suction line refrigerant enthalpy, q_{loss} is the compressor heat loss, α_{loss} is a heat loss ratio, and w_{pred} is the compressor specific work for normal operation which can be calculated from compressor map data for compressor power consumption ($\dot{W}_{map}$) and refrigerant mass flow rate ($\dot{m}_{ref,map}$) using Eq. (4). The heat loss ratio of low-side hermetic compressors used for packaged air conditioning equipment is typically small [9] and it is reasonable to assume a value of about 5% without sacrificing much accuracy (refer to Section 7). In addition, α_{loss} can then be tuned using real data when implementing the technique.

Using this model, the residual ΔT_{dis} between predicted $T_{dis,pred}$ and measured $T_{dis,meas}$ is only a function of compressor valve leakage independent of operating conditions and faults in other components. Fig. 3 shows the decoupling scheme. The residual ΔT_{dis} is only impacted by compressor faults and all the other factors including other component faults and overall system driving conditions have been taken into account by P_{suc}, T_{suc} and P_{dis}.

The faulty data sets collected by Breuker [8] were used to validate the models. Fig. 4 illustrates the discharge line temperature residuals for different fault types with different fault and load levels obtained using compressor power consumption and refrigerant mass flow rate determined from virtual sensors as described in subsequent sections. The terms "CompLeak", "CondFoul", "EvapFoul", "LLRestr" and "RefLeak" stand for compressor leakage fault, condenser fouling fault, evaporator fouling fault, liquid-line restriction fault and refrigerant leakage fault, respectively. Fault levels are numbered with increasing severity, with level one corresponding to "fault free". It can be seen that:

(1) The discharge temperature residuals ranged from 3 °C to 5 °C even when no fault was introduced. Through comparison with data collected by Rossi [14] from the same equipment it was determined that compressor performance had degraded due to extensive fault testing.
(2) Compressor valve leakage fault has a significant influence on the discharge temperature residual, whereas other faults have a much smaller impact on this performance indice. Some of the other faults can cause the discharge temperature residual to decrease at high fault levels where refrigerant entering the compressor is a two-phase mixture or has an overly high degree of superheat. Under these conditions, the virtual sensor used to determine refrigerant mass flow rate is less accurate. However, the residual has the opposite sign compared to compressor valve leakage and no errors in diagnosis will result.

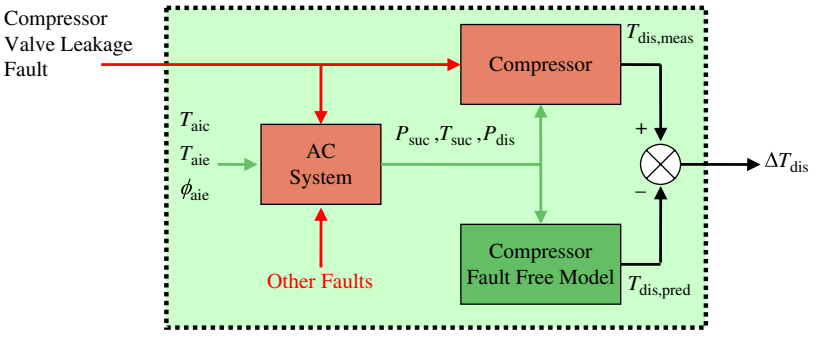

Fig. 3. Compressor valve leakage decoupling scheme.

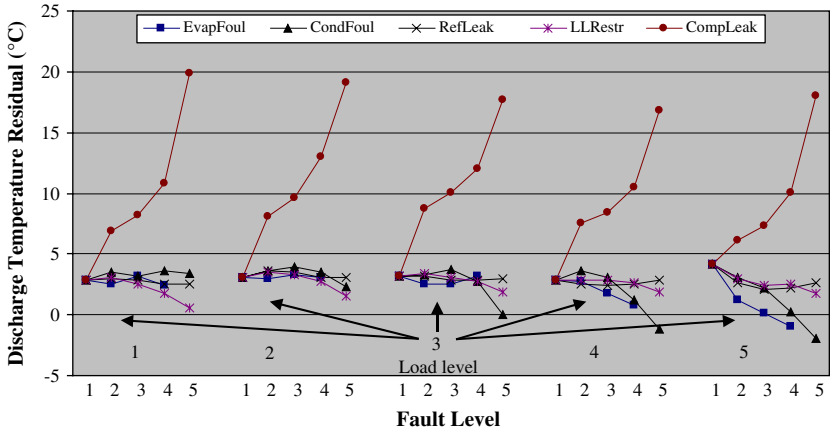

Fig. 4. Decoupling compressor valve leakage fault using virtual sensors for compressor power refrigerant mass flow rate to estimate discharge temperature residuals.

In summary, the coupling between compressor valve leakage and other faults is broken successfully using the discharge line temperature residual.

2.2. Virtual sensor for compressor power consumption

Compressor power consumption is an important parameter for monitoring equipment performance and calculating equipment efficiency, but it would be expensive to measure directly. Fortunately, compressor map data provided by manufacturers are readily available and can be used to estimate compressor power consumption when the compressor operates normally. According to ANSI/ARI Standard 540-1999, compressor manufacturer's map data can be represented using a 10-coefficient polynomial equation in the form of:

$$X = c_1 + c_2 S + c_3 D + c_4 S^2 + c_5 SD + c_6 D^2 + c_7 S^3 + c_8 DS^2 + c_9 SD^2 + c_{10} D^3 \quad (5)$$

where the c_i's are equation coefficients, S is suction dew point temperature (°C), D is discharge dew point temperature (°C), and X can be mass flow rate (kg s^{-1}), power consumption (kW), current (A), or compressor efficiency such as coefficient of performance (COP) and volume efficiency (η_v).

Although compressor map data are obtained when the compressor operates normally and at a constant suction superheat of 11 °C, a map will predict compressor power consumption with reasonable accuracy when the compressor deviates from the rating superheat conditions and even when there is an internal leakage fault. For a hermetic compressor, the power consumption is essentially related to compressor displacement, residual volume, inlet and outlet pressures, and efficiencies for compression, mechanical elements and the motor. Compressors used in unitary air conditioners are hermetic compressors and typically operate in a near-adiabatic condition. For a given compressor used in a unitary air conditioner,

(1) compressor displacement and residual volume are fixed and not affected by degradation faults;
(2) compression, mechanical and motor efficiencies are relatively constant and vary slightly with compression ratio. Degradation faults do affect compressor inlet and outlet pressures and thus compression ratio but hardly affect compression, mechanical and motor efficiencies directly.

Therefore, the primary sensitivity of compressor power consumption to valve leakage faults is due to their effects on compressor inlet and outlet pressures. Since a compressor map model uses compressor inlet and outlet pressures as inputs, it is expected to predict compressor power consumption at reasonable accuracy when the compressor has been degraded due to compressor valve leakage.

Data collected by Breuker [8] were used to validate this hypothesis. Fig. 5 plots predictions of a 10-coefficient power consumption polynomial model determined using manufacturers' data ($\dot{W}_{pred}$) vs. power consumption measurements ($\dot{W}_{meas}$) determined by Breuker from an operating air conditioner. Although these data were collected with no fault artificially introduced, the compressor performance had degraded due to extensive fault testing. Even with this fault, predictions match measurements very well and prediction error is within ±5%.

Fig. 6 shows compressor power consumption predictions ($\dot{W}_{pred}$) and measurements ($\dot{W}_{meas}$) for data collected with five different kinds of faults individually implemented (compressor leakage, condenser fouling, evaporator fouling, liquid-line restriction, and refrigerant undercharge). The predictions and measurements are within about 5%. The results are similar to those of Fig. 5 in that the model underpredicts slightly at low values and overpredicts a little for high

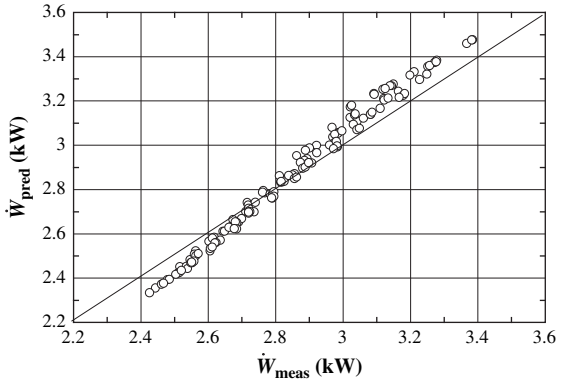

Fig. 5. Compressor power consumption predictions vs. measurements for ''normal operation''.

values. Overall, the agreement is good and a compressor power map determined from manufacturers' data can provide accurate estimates for faulty operation.

2.3. Virtual sensor for refrigerant flow

Refrigerant flow rate is needed for several virtual sensors, but would be too expensive to measure directly. For a normally operating compressor, manufacturer's data can be used to correlate flow rate in terms of suction conditions and discharge pressure. Rather than correlating mass flow rate directly, the data are used to calculate the volumetric efficiency of the compressor and then volumetric efficiency is correlated. Volumetric efficiency (η_v) is defined as the ratio of volumetric flow rate at the suction of the compressor to the volumetric displacement rate of the compressor. With this definition, the mass flow rate is,

$$\dot{m}_{ref,normal} = \eta_v \frac{NV}{v_{suc}} \tag{6}$$

where N is the number of suction strokes per unit time, V is the displacement volume, and v_{suc} is the suction line refrigerant specific volume.

The 10-coefficient Eq. (5) can be used to correlate volumetric efficiency determined from manufacturers' data and has good accuracy. However, Li and Braun [15] proposed the following empirical form for correlating volumetric efficiency that was employed in the current study

$$\eta_v = a_0 + a_1 \frac{P_{dis}}{P_{suc}} + a_2 \left(\frac{P_{dis}}{P_{suc}}\right)^2 + a_3 (T_{amb} - T_{suc})^{a_4} \tag{7}$$

where a_0, a_1, a_2, a_3 and a_4 are empirical coefficients, P_{suc} is suction pressure, P_{dis} is discharge pressure, T_{amb} is compressor ambient temperature, T_{suc} is suction temperature. If T_{amb} is not directly measured, it can be replaced with T_{aoc} (when the compressor is located in the condenser outlet air stream) or T_{aic} (when the compressor is not directly in the condenser outlet air stream).

Fig. 7 shows comparisons between measurements ($\dot{m}_{ref,meas}$) of Breuker [8] and predictions ($\dot{m}_{ref,pred}$) of mass flow rate determined using the empirical correlation model fit to manufacturer's data. Predictions of the empirical correlation model were about 7% higher than measurements because the compressor performance had deteriorated from extensive laboratory testing. Further analysis is provided in Section 7.

Unlike compressor power consumption, mass flow rate cannot be predicted using compressor map data when the compressor is faulty. Therefore, an alternative approach is proposed for a refrigerant mass flow rate virtual sensor that is based on the following compressor energy balance.

$$\dot{m}_{ref} = \frac{\dot{W} - \dot{Q}_{loss}}{h_{dis} - h_{suc}} \tag{8}$$

Compressor heat loss ($\dot{Q}_{loss}$) is generally quite small for packaged air conditioners and can be approximated as a constant fraction (α_{loss}) of $\dot{W}$. α_{loss} has been defined in Eq. (3)

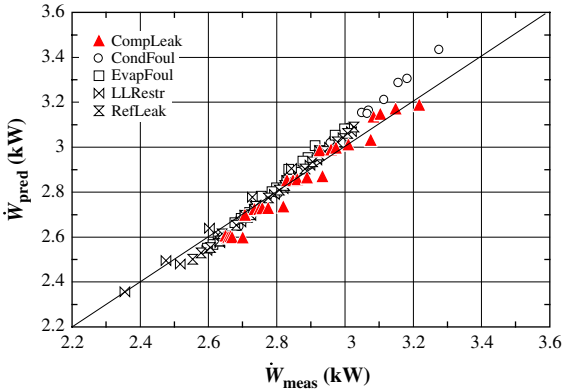

Fig. 6. Compressor power consumption predictions vs. measurements for faulty operation.

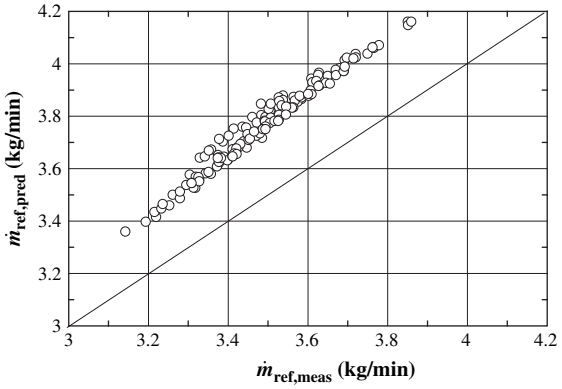

Fig. 7. Refrigerant flow rate predictions (by empirical model) and measurements.

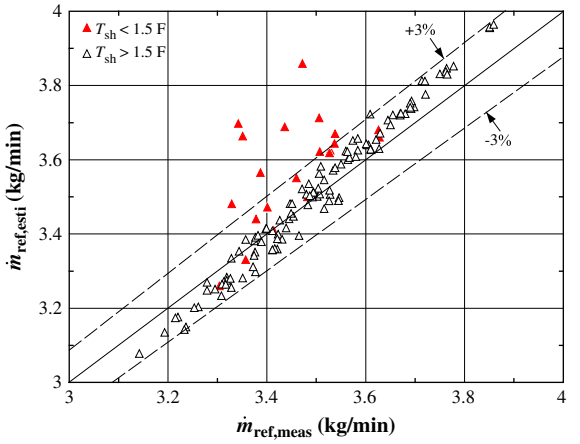

Fig. 8. Mass flow rate estimates using virtual sensor for "normal operation data".

and guidance about the choice for it has been provided therein. When combined with the virtual sensor for power consumption, Eq. (8) can be used as a virtual sensor to estimate refrigerant mass flow rate at both normal and faulty operations.

Fig. 8 compares estimates ($\dot{m}_{ref,esti}$) from the mass flow rate virtual sensor and measurements ($\dot{m}_{ref,meas}$) when no fault was introduced within the system. The mass flow rate estimates were determined using Eq. (8) with predictions from the power consumption virtual sensor and a heat loss fraction of 5%. Except for nine test points out of 135, the model estimates were within ±3% of the data. The larger errors for the nine conditions occurred when the measured superheat at the compressor inlet was below 1.5 °F. It is likely that there was a two-phase mixture entering the compressor under these conditions and leading to an inaccurate estimate of the suction enthalpy. The magnitude of the error depends on refrigerant quality.

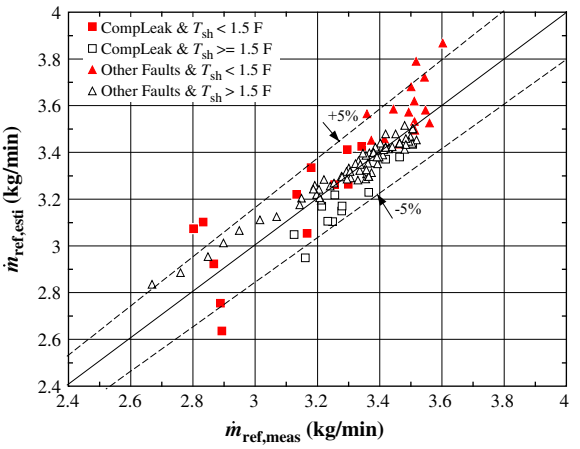

Fig. 9. Mass flow rate estimates using virtual sensors for faulty operation data.

Fig. 9 compares the mass flow rate estimates ($\dot{m}_{ref,esti}$) and measurements ($\dot{m}_{ref,meas}$) for a range of different faults at different fault levels. Except for several low superheat conditions, the virtual sensor works very well regardless of the fault.

It should be pointed out that although the virtual refrigerant mass flow rate sensor works well for both normal and faulty operations, the compressor map model may be more reliable and robust if the compressor operates normally. Under unfavorable conditions such as when two-phase or extremely high superheat refrigerant enters the compressor, the proposed virtual mass flow sensor may not be as reliable.

3. Condenser module

3.1. Decoupling feature for non-condensable gas

Air is a non-condensable gas that can be introduced through service for vapor compression systems that use typical refrigerants that operate at positive pressures. Ideally, this fault would be diagnosed and fixed by a service technician immediately after it is introduced to eliminate an additional service call. When mixed with a two-phase refrigerant, a non-condensable gas exerts a partial pressure that changes the relationship between the refrigerant saturation temperature and total pressure. After the system has running and is turned off, the non-condensable gas tends to accumulate in the condenser [16]. Therefore, when the system is off and two-phase refrigerant exists within the condenser, the difference between measured condensing temperature ($T_{cond,meas}$) and saturated temperature calculated from measured high side pressure ($T_{cond,pred} = t_{sat}(P_{dis})$), ΔT_{cond}, can be used as a decoupling feature for non-condensable gas.

Although it is possible to diagnose the presence of a non-condensable gas when the unit is running, turning the unit off eliminates spatial pressure variations within the high side of the system thereby reducing the importance of sensor location. The condensing temperature can be measured using an insulated sensor attached to a return bend in the middle of the condenser. The location is not that critical if the unit is off and two-phase refrigerant exists in the condenser. The discharge pressure can be measured at the discharge port of the compressor.

It is important to ensure that two-phase refrigerant exists within the condenser during the diagnosis of a non-condensable gas when the unit is off. This will generally be the case for a system with a thermal expansion device (TXV), since the TXV closes when the compressor stops. For a fixed-orifice system, liquid refrigerant will migrate to the evaporator under summer conditions where the condenser ambient is warmer than evaporator air. However, two-phase refrigerant will typically reside within the condenser for a sufficient period of time after the unit is turned off in order to allow diagnosis of a non-condensable gas.

Under conditions where the condenser ambient temperature is colder than the evaporator inlet air temperature, then two-phase refrigerant will exist in the condenser at steady state when the unit is off.

The sensitivity of ΔT_{cond} to the presence of a non-condensable gas can be demonstrated through the use of a simple model. Assuming that the refrigerant vapor and non-condensable gas form an ideal gas mixture, then it can be shown using Dalton's law that

$$\frac{P_{ncg}}{P_{dis}} = \frac{1}{1 + \frac{x_{ref}}{r_{ncg}}} \tag{9}$$

where P_{ncg} is the non-condensable gas partial pressure, x_{ref} is the quality or the mole fraction of vapor refrigerant in the refrigerant liquid–vapor mixture, r_{ncg} is the mole ratio of non-condensable gas to total refrigerant.

The Clapeyron Equation can be used to give

$$\Delta T_{cond} = \left(P_{ref,vapor} - P_{dis}\right)\frac{T_{cond,meas} v_{fg}}{h_{fg}} \tag{10}$$

where $P_{ref,vapor}$ is the refrigerant partial pressure (saturation pressure at $T_{cond,meas}$), h_{fg} is the enthalpy of vaporization $h_g - h_f$, v_{fg} is specific volume change ($v_g - v_f$), and $T_{cond,meas}$ is the measured condensing temperature on an absolute temperature scale.

Eqs. (9) and (10) can be combined to give

$$\Delta T_{cond} = \frac{-r_{ncg}}{x_{ref}}\left(\frac{P_{ref,vapor} v_{fg}}{h_{fg}}\right) T_{cond,meas} \tag{11}$$

For an air conditioning application employing R22, the term in brackets on the right-hand side of Eq. (11) has a value of approximately 0.13 at typical condensing conditions. In this case,

$$\Delta T_{cond} = -0.13\,\frac{r_{ncg}}{x_{ref}}\,T_{cond,meas} \tag{12}$$

where $T_{cond,meas}$ is measured on an absolute temperature scale.

The feature ΔT_{cond} is very sensitive to non-condensable gas when there is a two-phase mixture in the condenser. However, it is also very sensitive to refrigerant quality in the condenser. Tables 1 and 2 show estimates of ΔT_{cond} for different ambient temperatures and refrigerant charges for a system that is off and has 30 kPa of non-condensable gas. Table 3 shows estimates of ΔT_{cond} for various amount of non-condensable gas under normal charge and at an ambient temperature of 30 °C. These estimates were determined from Eq. (12) using measurements obtained by Breuker [8] and Harms [9] for packaged air conditioners using R22. The sensitivity of ΔT_{cond} to the presence of the non-condensable gas is reduced as refrigerant charge decreases and/or ambient temperature increases. However, the sensitivity is excellent for diagnosing this fault under most realistic conditions.

Table 1
x_{ref} and ΔT_{cond} with nominal charge and 30 kPa of non-condensable gas

T_{amb} (°C)	20	30	40
ΔT_{cond} (°C)	7.0	5.7	4.8

Table 2
ΔT_{cond} with $T_{amb} = 30$ °C and 30 kPa of non-condensable gas

Charge level	40%	60%	80%	90%	100%	110%	120%
$\Delta T_{cond,abnorm}$ (°C)	2.2	2.7	3.7	4.5	5.7	7.8	12.6

3.2. Decoupling feature for condenser fouling

A packaged air conditioning system typically uses a constant-speed fan with ambient air to cool condenser coils. Fouling mainly develops on the air side and affects heat transfer in two ways [17,18]. First of all, fouling caused by small-scale dirt can impact air-side heat transfer coefficients directly by providing an insulating resistance (heat transfer is reduced) and also through its affect on local air flow patterns (heat transfer is enhanced); overall, the heat transfer can be either enhanced or reduced. The second, and more significant, effect of fouling is reduced air flow area which results in increased pressure drop and reduced air flow rate and is caused by both small- and large-scale deposits. Because of its large sensitivity to fouling of any kind, condenser air flow rate reduction is an excellent independent feature for condenser fouling. It also is a good feature for diagnosing condenser fan problems. Other features that characterize the overall condenser conductance for heat transfer are not nearly as good because they may have a smaller sensitivity to air-side fouling and are dependent on refrigerant-side flow rates and conditions.

It is too expensive and unreliable to measure condenser air flow directly. Therefore, it is determined from a virtual sensor that employs a steady-state energy balance and other available measurements. From an energy balance on the condenser,

$$\dot{V}_{ca} = \frac{v_{ca}}{C_{p,air}}\,\frac{\dot{m}_{ref}\left(h_{dis}(P_{dis}, T_{dis}) - h_{ll}(P_{ll}, T_{ll})\right)}{\left(T_{aoc} - T_{aic}\right)} \tag{13}$$

where $\dot{V}_{ca}$ is condenser air volume flow rate, v_{ca} is condenser air specific volume, $C_{p,air}$ is air specific heat, T_{aoc} is condenser outlet air temperature, T_{aic} is condenser inlet air

Table 3
ΔT_{cond} with $T_{amb} = 30$ °C and various amount of non-condensable gas

Condensable gas pressure (kPa)	5	15	30	60	90
$\Delta T_{cond,abnorm}$ (°C)	1.0	2.8	5.7	11.4	17.1

temperature, $\dot{m}_{ref}$ is refrigerant mass flow rate, h_{dis} is discharge line refrigerant enthalpy, P_{dis} is discharge line pressure, T_{dis} is discharge line temperature, h_{ll} is liquid-line refrigerant enthalpy, and T_{ll} is liquid-line temperature.

Eq. (13) assumes that the refrigerant is subcooled at the outlet of condenser. If it is not subcooled, then a fault is most likely present, which the FDD system should detect and diagnose.

Eq. (13) is a virtual sensor for condenser air volume flow rate $\dot{V}_{ca,meas}$. The refrigerant mass flow rate is determined from a virtual sensor as described in the compressor module section and all the other parameters on the right-hand side of Eq. (13) can be determined from low-cost measurements. The normal model for $\dot{V}_{ca}$ would be a constant value for a fixed-speed condenser fan. Practically, the normal value of $\dot{V}_{ca}$ would be learned when the FDD scheme is implemented assuming that there is no fouling.

In order to evaluate refrigerant properties, it is necessary that there be no non-condensable gas in the system. This assumption is reasonable because the non-condensable gas fault can be excluded immediately after service is done. Fig. 10 illustrates the decoupling scheme for condenser fouling and non-condensable gas faults.

Fig. 11 shows the condenser volume flow rate estimated from Eq. (13) using a refrigerant mass flow rate determined from a virtual sensor for different fault types with different fault and load levels. The estimated condenser volume flow rate is primarily influenced by condenser fouling. The only significant errors in predicted condenser air flow occur at the high levels of compressor valve leakage under high load levels. This error is caused by errors in virtual refrigerant mass flow prediction due to two-phase refrigerant entering the compressor. Fortunately, the FDD method can diagnose a compressor leakage fault at very low levels, so practically this would not be a problem.

3.3. Virtual sensor for condenser exit (liquid-line inlet) pressure

The condenser outlet pressure (liquid-line inlet pressure) is needed for determination of several variables, including properties for the virtual condenser air flow sensor, condenser subcooling for the refrigerant charge feature, and inlet pressure for the liquid-line restriction feature. The refrigerant exiting the condenser is typically subcooled at a pressure that is somewhat lower than the pressure exiting the compressor. Under these conditions, the simplest approach for estimating this pressure when the compressor discharge pressure is measured involves neglecting the condenser pressure drop or assuming a constant pressure drop across the condenser. For packaged air conditioners, the pressure drop across the condenser and discharge line ranges from 100 kPa to 240 kPa.

A somewhat better estimate is possible if the condensing temperature can be measured near the condenser outlet. Then the pressure can be determined from saturation properties at that temperature ($P_{ll} \approx p_{sat}(T_{cond})$), where $p_{sat}(\,)$ is the refrigerant saturated pressure function. In order to estimate the condensing temperature cost effectively, a single sensor could be surface mounted to a return bend within the condenser where two-phase refrigerant is most often present under steady-state conditions. The sensor should be insulated from the ambient and located at the point where different condensing circuits are combined. It is possible for the refrigerant at this point to have a small degree of subcooling if there is a severe liquid-line restriction or if the unit is overcharged with refrigerant. However, a small degree of subcooling would have a small impact on the estimated pressure. On the contrary, 0.5–1.0 °C subcooling would compensate for the error resulting from neglecting the pressure drop in the condenser subcooling section. For example,

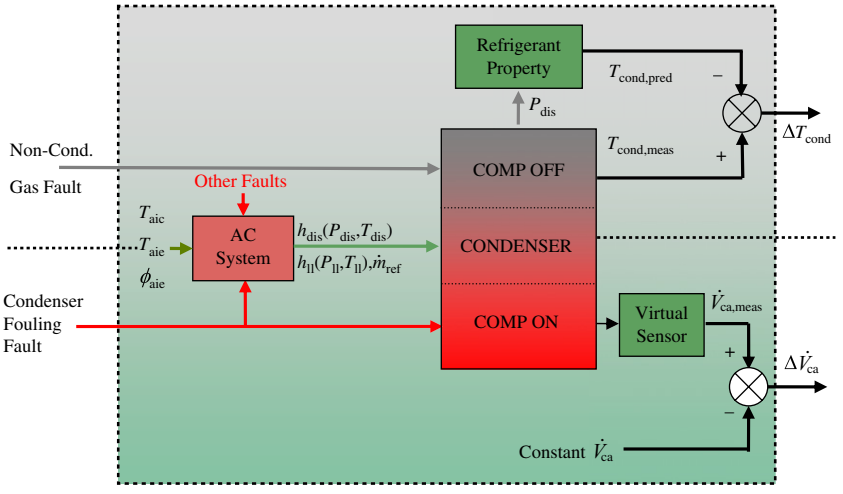

Fig. 10. Condenser fouling and non-condensable gas faults decoupling scheme.

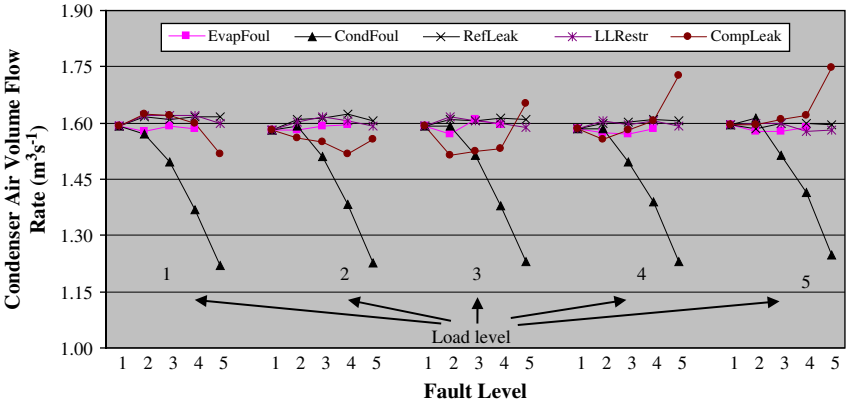

Fig. 11. Decoupling condenser fouling fault using estimated refrigerant mass flow rate.

a 2 °C degree of subcooling results in about a 30 kPa error in pressure.

4. Expansion module – decoupling feature for liquid-line restriction

Packaged air conditioners often include a filter/dryer to protect the expansion device and compressor from contaminants. When the filter/dryer is loaded with water and/or dirt, there is a significant pressure drop (ΔP_{ll}) and the device no longer functions properly and should be replaced. A measurement of the pressure drop across the filter/dryer would be too expensive and is not practical. Therefore, virtual sensors are employed to estimate the pressure drop from lower cost measurements.

Fig. 12 depicts the decoupling scheme and input requirements for the virtual sensors and shows the location of the relevant state variables and relevant components. The inputs to the virtual sensors include measurements and outputs from other virtual sensors that are necessary for two different approaches that have been developed for estimating the inlet and outlet pressures. One approach is appropriate when the unit is operating under quasi-steady conditions. The other method utilizes measurements obtained during a startup transient for the unit. The two approaches can be combined to provide reliable diagnoses for a wide variety of conditions and systems.

4.1. Virtual sensors under quasi-steady conditions

Under quasi-steady conditions, the liquid-line inlet pressure is estimated using the virtual sensor described within the condenser module. The virtual sensor for inlet pressure to the expansion device is more complicated and depends on whether the refrigerant is a subcooled liquid or a two-phase mixture.

For a small degree of condenser subcooling and/or a large pressure drop across the liquid line, the condition of the refrigerant exiting the liquid line could be two-phase. In this case, the pressure can be estimated from a temperature measurement using saturation properties ($P_x = p_{sat}(T_x)$). A two-phase condition can be detected by monitoring the temperature difference across the liquid line. If the refrigerant is subcooled throughout, then the temperature difference will be not observable. Conversely, the temperature difference is very sensitive to pressure drop for a two-phase mixture.

For a typical degree of condenser subcooling, the pressure drop across the liquid line would need to be very significant in order to effect a change of phase. Consider an example for R22 with a condensing temperature of 50 °C

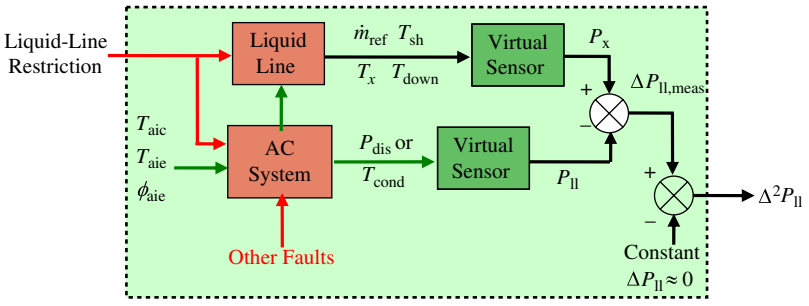

Fig. 12. Liquid-line restriction decoupling scheme.

and 8 °C of subcooling. The pressure drop resulting from a restriction would need to be larger than about 333 kPa to reach a saturation condition. An additional pressure drop of about 100 kPa would be necessary for a 3 °C temperature drop. In addition, the presence of a liquid-line restriction would lead to an increase in condenser subcooling for systems with fixed expansion devices, compounding the difficulty in early diagnosis of this fault.

Under more typical conditions, the refrigerant exiting the liquid line is a subcooled liquid. Li and Braun [12] developed a method to estimate P_x through modeling the expansion device. For a fixed orifice, the pressure drop across the orifice ($P_x - P_{down}$) is a function of refrigerant mass flow rate and refrigerant subcooling entering the orifice. Since the refrigerant mass flow rate can be estimated using a virtual sensor and the orifice outlet pressure (P_{down}) is the saturated pressure of the orifice outlet temperature (T_{down}), the orifice inlet pressure can be obtained. With P_x and P_{ll} estimated, the pressure drop across the filter/drier can be calculated. Fig. 13 shows the estimated pressure drop across the filter/drier under different fault types with different fault and load levels using estimated pressures before and after the filter/drier. It can be seen that the liquid-line pressure drop is dominantly influenced by a liquid-line restriction fault. The coupling between liquid-line restriction faults and all other faults is broken successfully.

4.2. Virtual sensors under transient conditions after startup

More accurate and simpler estimates of liquid-line pressure drop can be obtained using startup transients for vapor compression equipment. For significant periods of time (up to 4 min) during this transient, refrigerant at the inlet and exit of the liquid line exists as a two-phase mixture. This situation can be detected by monitoring the subcooling exiting the condenser. When condenser subcooling is close to zero, entering and leaving pressures can be accurately determined from temperatures and saturation properties according to

$$\Delta P_{ll} = p_{sat}(T_x) - p_{sat}(T_{ll}) \tag{14}$$

Transient tests have been performed on a number of systems incorporating TXV and fixed-orifice expansion devices in order to confirm the validity of this approach. Fig. 14 shows transient measurements of liquid-line temperature and pressure, condenser subcooling, and condenser air temperature difference after startup for a heat pump having a TXV with no liquid-line restriction. Prior to the system turning on, the refrigerant in the condenser is most likely a saturated mixture because the TXV traps high-pressure refrigerant in the condenser. After the compressor starts, it takes some time for the TXV to open and therefore all the compression work is converted into internal energy and both the liquid-line pressure and temperature increase rapidly. The indicated subcooling also increases dramatically, but it is not possible to get an accurate liquid-line temperature measurement during this period because there is no refrigerant flow. After the TXV opens, the pressure drops rapidly while the liquid-line temperature keeps increasing so the overall impact is that the condenser subcooling goes to zero. After all the refrigerant residing in the condenser initially is purged out and hot fresh refrigerant from the compressor begins to circulate, both the refrigerant pressure and liquid-line temperature increase but with a decreasing slope over time. This is because part of compression work is converted into kinetic energy and the air-side heat transfer is enhanced with the condenser surface's temperature picking up gradually. It can be seen that the profile of liquid-line temperature has a similar shape as the air temperature difference across condenser except for a 5-s delay. Liquid-line refrigerant temperature tends to increase for about 4 min along with the condensing pressure and temperature. During these 4 min, the refrigerant quality at the exit of the condenser decreases from 1 to 0. After 4 min, the

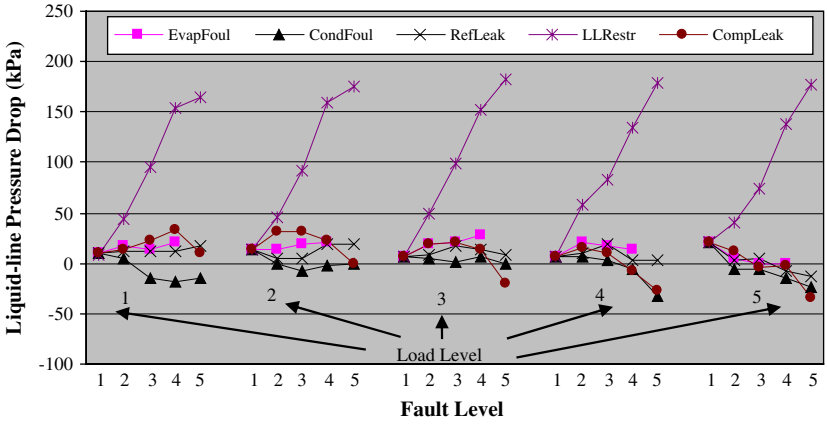

Fig. 13. Decoupling liquid-line restriction using estimated pressure drop.

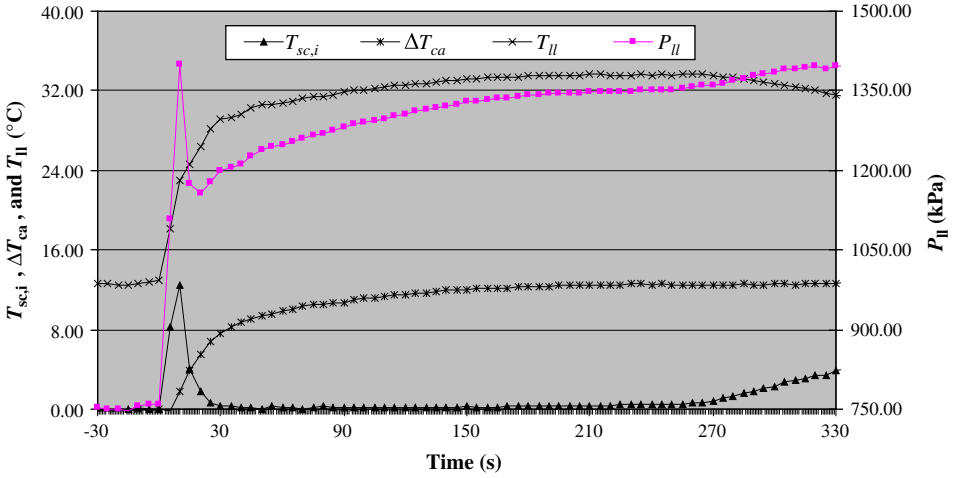

Fig. 14. Transient changes in state variables for a system with a TXV and no liquid-line restriction fault.

condensing temperature and pressure continue to increase but increasing condensing temperature tends to enhance heat transfer and leads to refrigerant subcooling at the exit of condenser. However, the increased subcooling leads to less heat transfer surface for two-phase heat transfer. These two compensating factors eventually reach a balance point and the subcooling approaches a quasi-steady value. The transient for condenser air temperature difference is better behaved and appears to approach a quasi-steady condition more quickly than the liquid-line pressure and temperature. The length of time shown in Fig. 14 was not sufficient for the liquid-line pressure and subcooling to achieve quasi-steady conditions.

In summary, for the TXV system, the liquid-line subcooling profile consists of four stages: (1) at the beginning, it increases suddenly to a peak during a very short period of time (about 10 s); (2) it drops from the peak suddenly to zero during another very short period of time (about 10 s); (3) it remains at zero for a significant period of time (about 4 min); (4) finally, it begins to increase gradually until reaching steady-state.

During the 4 min when the subcooling remains close to zero, virtual pressure sensors could utilize two-phase temperature measurements to determine liquid-line pressures. Although these data were collected from a split system with a 3-m long liquid line, the conclusion can be safely generalized to packaged systems. The velocity of refrigerant in the liquid line ranges from 0.67 m s^{-1} (liquid refrigerant) to 10 m s^{-1} (vapor refrigerant). Compared to 4 min, the time for the refrigerant to go through the liquid line is on the scale of from a fraction of a second to several seconds and is negligible.

Fig. 15 shows measured subcooling for the refrigerant entering and leaving the liquid line, measured pressure and temperature drop across the liquid line, and virtual pressure drop determined from temperature measurements. Since there is no restriction, the liquid-line temperature difference

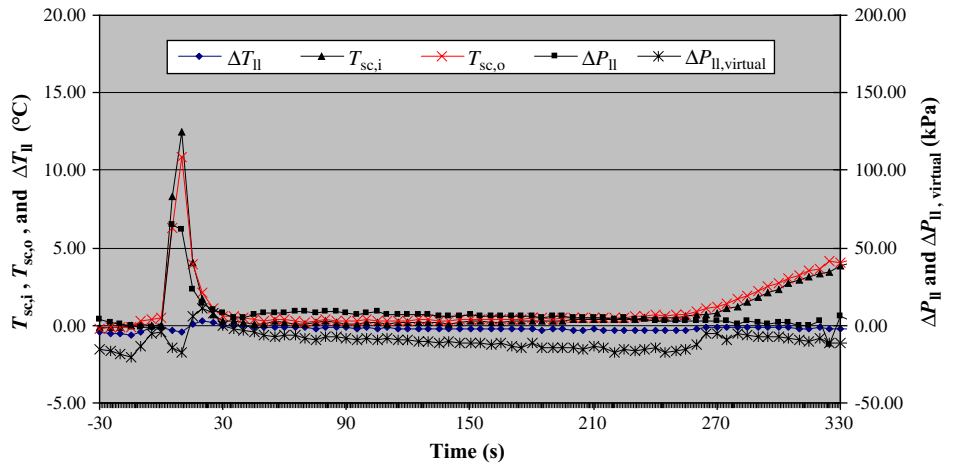

Fig. 15. Transient changes in state variables for a system with a TXV and no liquid-line restriction fault.

is close to zero regardless of whether the refrigerant is subcooled or two-phase. The pressure drop virtual sensor readings are close to zero and no restriction fault diagnosis is triggered. However, the virtual sensor should only be enabled when the subcooling is close to zero.

Fig. 16 plots the startup profiles for the same variables shown in Fig. 15 when there is a liquid-line restriction fault causing about 120 kPa pressure drop. It can be seen that there is a significant temperature drop across the filter/dryer during the startup period. The temperature drop across the filter/dryer increases suddenly once the residual refrigerant in the condenser has been purged. After the temperature drop reaches its peak, it drops gradually instead of remaining flat due to the following reason. With the existence of a restriction fault, the system performance is impacted including startup performance. As illustrated in Figs. 14 and 15, the filter/dryer upstream subcooling remains two-phase flow for a significant period of time during the startup when there is no restriction fault. However, the restriction fault tends to increase the filter/dryer upstream subcooling so the two-phase flow period is shortened from about 4 min to 2 min. Since the upstream subcooling increases gradually, a significant temperature drop can be seen during its subsequent low-subcooling period (2 min). It demonstrated that the virtual pressure sensor can identify the restriction fault during the 4-min transient period.

Although the startup transients are somewhat different for systems that employ fixed expansion orifices (FXO), the period of time associated with two-phase refrigerant entering and leaving the liquid line is quite similar. For a FXO system, since the FXO is always open the liquid-line pressure profile is different than that of a TXV system at the beginning two stages (a period of around 20 s). During the first 10 s, the refrigerant pressure value increase suddenly to a lower value than that of a TXV system. During the second 10 s, the refrigerant pressure keeps increasing instead of decreasing. After the beginning 20 s, the pressure has a similar profile to a TXV system. Unlike the pressure, the refrigerant temperature for a FXO system has a similar startup profile to a TXV system. Overall, the subcooling profile for a FXO system is similar to a TXV system. Therefore, transient temperature data can be used for estimating liquid-line pressure drop for both TXV and FXO systems.

5. Evaporator module

5.1. Decoupling feature for evaporator fouling

Similar to condenser fouling, evaporator or evaporator filter fouling develops on the air side and the dominant impact is a reduction in air flow rate. Evaporator air flow reduction can also be caused by improper fan settings or fan or damper faults that occur during operation. Therefore, evaporator air flow rate reduction is an excellent feature for evaporator fouling or other causes of low air flow. Evaporator air flow is determined from a virtual sensor that employs an energy balance and other available measurements according to

$$\dot{V}_{ea} = \frac{v_{ea}\dot{m}_{ref}(h_{suc}(P_{suc}, T_{suc}) - h_{ll}(P_{ll}, T_{ll}))}{h_{aie}(T_{aie}, \phi_{aie}) - h_{sa}(T_{aoe}, \phi_{aoe})} \quad (15)$$

where $\dot{V}_{ea}$ is evaporator air volume flow rate, v_{ea} is evaporator air specific volume, h_{sa} is the evaporator outlet air enthalpy, ϕ_{aoe} is the relative humidity of evaporator outlet air, T_{aoe} is evaporator outlet air temperature, h_{aie} is evaporator air inlet enthalpy, T_{aie} is evaporator inlet air temperature, ϕ_{aie} is the relative humidity of evaporator inlet air, h_{suc} is suction line refrigerant enthalpy, P_{suc} is suction line pressure, and T_{suc} is suction line temperature.

Eq. (15) is a virtual sensor or observer for measuring $\dot{V}_{ea,meas}$. Fig. 17 illustrates the decoupling scheme. Unlike

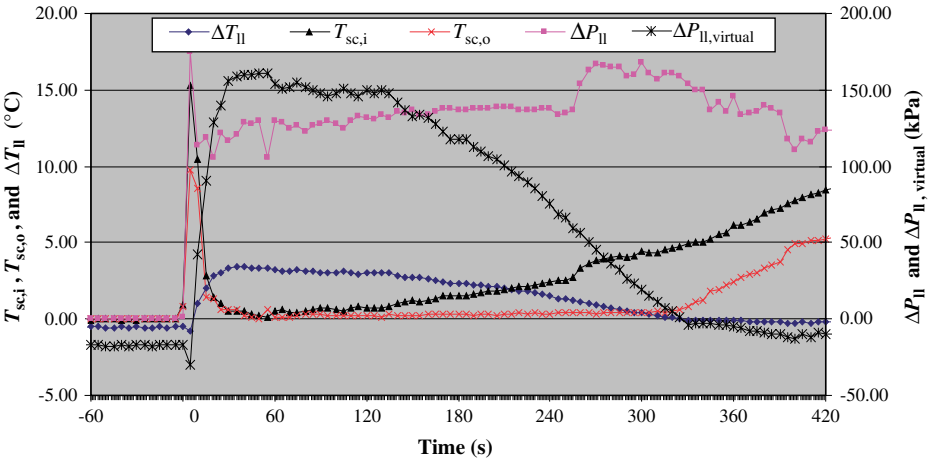

Fig. 16. Transient changes in state variables for a system with a TXV and a liquid-line restriction fault.

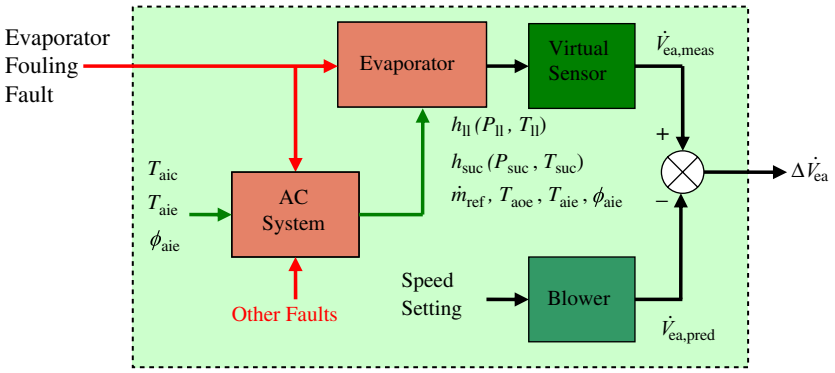

Fig. 17. Evaporator fouling decoupling scheme.

condenser air volume flow rate, $\dot{V}_{ea,pred}$ normally has more than one speed setting, but it is constant for a given setting. So, the block 'blower' acts as a normal model, whose input is the setting control signal and whose output is a constant air volume flow rate, $\dot{V}_{ea,pred}$, corresponding to the speed setting. Practically, the actual value of $\dot{V}_{ea,pred}$ would be learned when the FDD scheme is implemented with the assumption of no fouling.

Fig. 18 gives evaporator air volume flow rates estimated using a virtual sensor under different fault types with different fault and load levels. As expected, the evaporator air volume flow rate estimates are not good when there are severe compressor leakage faults and high load levels. At these conditions, two-phase refrigerant enters the compressor and the virtual refrigerant mass flow rate sensor provides inaccurate predictions. However, the evaporator air mass flow rate estimate is more sensitive to evaporator fouling than compressor valve leakage and the trend is the opposite (air flow estimates increase with compressor valve leakage). Furthermore, the FDD technique can diagnose compressor leakage faults at low levels, so practically this would not be a problem.

5.2. Virtual sensor for exit air humidity

The virtual sensor defined by Eq. (15) requires the humidity of the air exiting the evaporator coil. Typically, return and outdoor air humidities are measured for economizers but supply air humidity is not. The cost of this additional sensor can be avoided through the use of a virtual sensor. A supply air humidity virtual senor was developed using the bypass factor method. The bypass factor, BF, is defined as [19],

$$\mathrm{BF} = \frac{h_{aoe} - h_{s,evap}}{h_{aie} - h_{s,evap}} = \frac{w_{aoe} - w_{s,evap}}{w_{aie} - w_{s,evap}} \tag{16}$$

where h_{aoe}, h_{aie}, and $h_{s,evap}$ are evaporator outlet air (supply air) enthalpy, evaporator inlet air (mixed air) enthalpy and saturated air enthalpy at the evaporator surface temperature ($T_{s,evap}$), respectively; w_{aoe}, w_{aie}, and $w_{s,evap}$ are supply air humidity ratio, evaporator inlet air (mixed air) humidity ratio and saturated air humidity ratio at the evaporator surface temperature ($T_{s,evap}$), respectively. Fig. 19 illustrates the bypass factor analysis on a psychrometric chart.

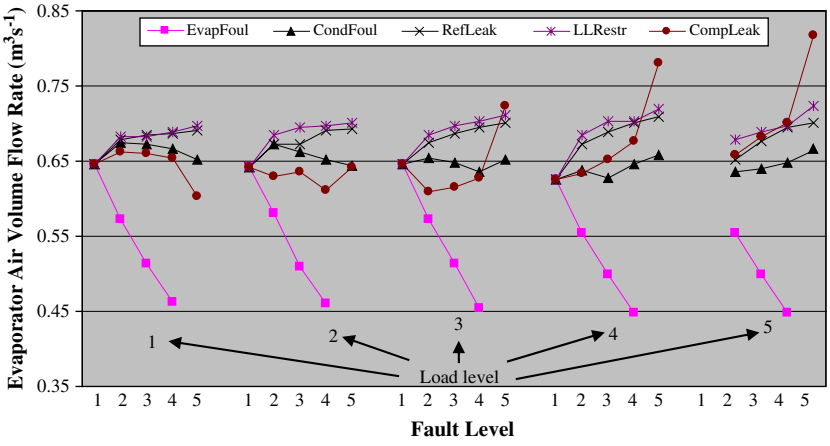

Fig. 18. Decoupling evaporator fouling fault using estimated refrigerant mass flow rate.

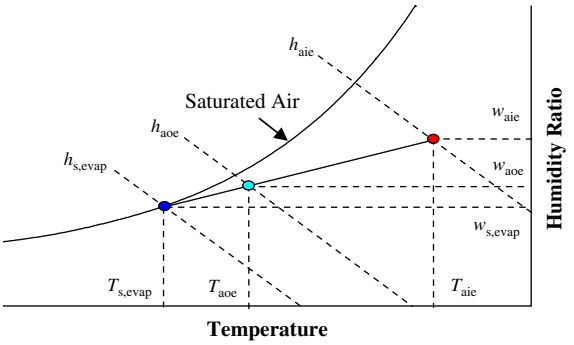

Fig. 19. Illustration of bypass factor analysis.

It can be shown that,

$$\frac{w_{aoe}-w_{s,evap}}{w_{aie}-w_{s,evap}}=\frac{T_{aoe}-T_{s,evap}}{T_{aie}-T_{s,evap}} \tag{17}$$

where T_{aoe} and T_{aie} are supply air temperature and mixed air temperature, respectively. Substituting Eq. (17) into (16),

$$\mathrm{BF}=\frac{T_{aoe}-T_{s,evap}}{T_{aie}-T_{s,evap}} \tag{18}$$

Since T_{aoe}, T_{aie}, and $T_{s,evap}$ are measured, BF can be calculated by Eq. (18). Rearranging Eq. (16),

$$w_{aoe}=\mathrm{BF}\left(w_{aie}-w_{s,evap}\right)+w_{s,evap} \tag{19}$$

Eq. (19) can be used as a virtual sensor for estimating w_{aoe}. Similarly, h_{aoe} can be estimated by the following equation,

$$h_{aoe}=\mathrm{BF}\left(h_{aie}-h_{s,evap}\right)+h_{s,evap} \tag{20}$$

5.3. Virtual sensor for evaporation temperature

The evaporation temperature is needed for determining suction superheat and the pressure entering the expansion device. If the compressor suction pressure is measured, then the evaporating temperature can be determined using saturation properties. However, this pressure sensor could be eliminated by a direct measurement of evaporating temperature using a single sensor surface mounted to a return bend. The sensor should be insulated from the ambient and located near the entrance of the evaporator.

6. Charge module – decoupling feature for high or low refrigerant charge

This section addresses relationships among the three system-level faults: refrigerant overcharge, refrigerant undercharge and refrigerant leakage. Although these three faults are system-level faults, from the classification criteria of fault cause, refrigerant overcharge and undercharge faults are service faults while refrigerant leakage is an operational fault. Service faults only happen during service and fault severity would not change over time, while operational faults normally develop during operation and they would become progressively worse over time. This information contributes to the development of an FDD technique for these faults.

From the viewpoint of fault effect, refrigerant undercharge and refrigerant leakage have the same fault effect on the system, low or deficient refrigerant charge, so they can be considered as a single fault when doing fault detection and then can be separated using the fault cause criteria when doing fault diagnosis. Physically, refrigerant deficient and excessive charge faults would not happen simultaneously, so there is no coupling among the three system-level faults for fault detection and it is easy to separate them using the fault cause criteria for fault diagnosis.

So far, couplings among system-level faults and between system-level faults and component-level faults have been broken. However, it is necessary to identify a feature that is uniquely related to the system charge inventory. Li and Braun [20] developed a feature for refrigerant charge that is expressed as

$$\Delta T_{sc-sh}=\left(T_{sc}-T_{sc,rated}\right)-\frac{k_{sh}}{k_{sc}}\left(T_{sh}-T_{sh,rated}\right) \tag{21}$$

where $T_{sc,rated}$ and $T_{sh,rated}$ are the system subcooling and superheat at the standard rating condition for the air conditioner and the ratio k_{sh}/k_{sc} is the slope of a straight line plot of $(T_{sc}-T_{sc,rated})$ vs. $(T_{sh}-T_{sh,rated})$ for the rated refrigerant charge. Theoretically, it is only necessary to have measurements of superheat and subcooling at the rating condition and a second operating condition to determine the ratio k_{sh}/k_{sc} for a given unit. It does not matter what conditions were changed in order to effect a change in subcooling and superheat (e.g., a change in condenser inlet temperature or flow rate, evaporator inlet temperature, humidity, or flow rate, or any combination of these variables). However, practically, Li and Braun [20] demonstrated that a change in condenser inlet temperature is the best condition under which k_{sh}/k_{sc} is evaluated and described a robust method for determining k_{sh}/k_{sc} for a given unit.

The refrigerant charge feature of Eq. (21) is relatively independent of operating conditions and almost uniquely dependent on refrigerant charge. It is positive for refrigerant overcharge and negative for undercharge. The magnitude of the deviation from zero is an indication of the level of the fault. Furthermore, it applies to systems with either fixed area or variable expansion devices.

Fig. 20 shows an example plot of the charge diagnostic feature as a function of refrigerant charge for different indoor and outdoor conditions. This feature has a value near zero for the nominal charge and decreases with decreasing charge. In addition to providing a feature for fault detection and diagnostics, this parameter provides a direct indication of the level of charge.

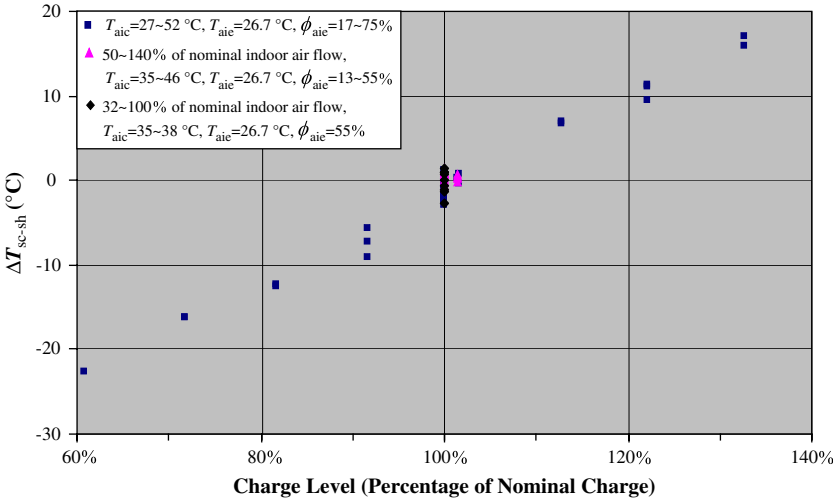

Fig. 20. ΔT_{sc-sh} vs. refrigerant charge levels for a split air conditioner with TXV as the expansion device and R410a as the refrigerant.

7. Uncertainty propagation analysis

Measured variables have a random variability which is referred as uncertainty. Outputs from virtual sensors also have uncertainties due to uncertainties in measured quantities and their propagation through models. The method described in National Institute of Standards and Technology (NIST) Technical Note 1297 [21] was adopted for determining this uncertainty propagation.

The measured variables used for the proposed virtual sensors are temperatures and pressures. Temperature measurements typically have an accuracy of ±0.5 °C. The absolute accuracy for pressure measurements depends on the full scale (FS) of the pressure sensor in that pressure sensors typically have a relative accuracy of ±0.5%–±1% FS. Since suction pressure sensors typically have a smaller full scale than discharge pressure sensors, the absolute accuracies of ±15 kPa and ±30 kPa are assigned to suction pressure measurements and discharge pressure measurements, respectively. The proposed virtual sensors also use compressor map data as an input. According to the ANSI/ARI Standard 540 [22], a relative accuracy of ±5% is assumed for refrigerant mass flow rate and power consumption data. The compressor heat loss ratio (α) for unitary air conditioning equipment is typically small, ranging from 0% to 10%. A constant value of 0.05 and an uncertainty of ±0.05 are

Table 4
Uncertainty analyses of virtual sensor outputs

Virtual sensor	Inputs (uncertainty)	Uncertainty
Compressor power consumption, $\dot{W}$	P_{suc} (±15 kPa), P_{dis} (±30 kPa), compressor map data (±5%)	±5.2%
Mass flow rate, $\dot{m}_{ref}$ (using compressor map)	P_{suc} (±15 kPa), P_{dis} (±30 kPa), T_{suc} (±0.5 °C), T_{amb} (±0.5 °C), compressor map data (±5%)	±6.4%
Mass flow rate, $\dot{m}_{ref}$ (using energy balance)	P_{suc} (±15 kPa), P_{dis} (±30 kPa), T_{suc} (±0.5 °C), T_{dis} (±0.5 °C), $\dot{W}$ (±5.2%), compressor heat loss ratio α (±0.05)	±7.5%
Discharge line temperature, $T_{dis,pred}$	P_{suc} (±15 kPa), P_{dis} (±30 kPa), T_{suc} (±0.5 °C), T_{amb} (±0.5 °C), compressor map data (±5%), compressor heat loss ratio α (±0.05)	±2 °C
Condensing temperature, T_{cond}	P_{cond} (±30 kPa),	±0.8 °C
Upstream pressure of expansion device, P_{up} (using expansion device model)	P_{ll} (±30 kPa), T_{ll} (±0.5 °C), T_{down} (±0.5 °C), $\dot{m}_{ref}$ (±7.5%)	±70 kPa
Upstream pressure of expansion device, P_{up} (using transient temperatures)	T_{ll} (±0.5 °C)	±20 kPa
Evaporator exit air humidity, ϕ_{aoe}	T_{aie} (±0.5 °C), ϕ_{aie} (±0.05), T_{aoe} (±0.5 °C), $T_{s,evap}$ (±0.5 °C),	±0.05

assumed. In summary, Table 4 tabulates all the assumed uncertainties in both directly and indirectly measured quantities used for model inputs.

Based on the above assumptions, uncertainty analyses for various virtual sensors were performed and are summarized in Table 4. The uncertainty values tabulated in Table 4 are similar to results presented in earlier sections. Figs. 5 and 6 show that the estimation error of compressor power consumption is within ±5%, while the uncertainty propagation analysis yields an error of ±5.2%. Fig. 7 suggests that there is a bias error of +7% using a compressor map model but the error propagation analysis indicates that the error should be within ±6.4%. The error of +7% is a systematic error caused by the compressor deterioration due to extensive laboratory testing. If the systematic bias error of +7% was removed, the pure random error is within ±3%. Fig. 8 shows that mass flow rate estimates obtained from an energy balance model had an error of ±3% when the state entering the compressor was known (i.e., not two-phase). This is consistent with the random error component of compressor map model but is much less than the error of ±7.5% obtained from the error propagation analysis. It appears that uncertainties in the inputs for the energy balance mass flow rate model were overestimated. For example, the uncertainty of $\dot{W}$ was assumed to be ±5.2% but the real data have less errors; the compressor map data was assumed to have an uncertainty of ±5% but extensive laboratory data from almost ten compressors indicated that compressor power consumption and mass flow rate data have an error of less than ±5%. Table 4 shows that the transient model for pressure estimation has a much higher accuracy than the expansion device model approach. The transient model has a much shorter error propagation channel than the expansion device model.

8. Conclusions

Several unique decoupling features and virtual sensors were developed and evaluated that allow low-cost implementation of an FDD method for vapor compression systems that handles multiple-simultaneous faults. The overall technique can be implemented with nine temperature sensors, two pressure sensors, and one humidity sensor. It is possible to replace the pressure sensors with temperature sensors if they are properly located. Any individual feature could be utilized on its own to provide a more limited FDD system. For instance, the decoupling feature for refrigerant charge could be used in a stand-alone system for diagnosing refrigerant leakage or refrigerant undercharge or overcharge after service. Li and Braun [23] described implementation of the method and present experimental and field evaluation results of its performance. The method presented in this paper was developed and validated for simple vapor compression systems having fixed-speed fans and on/off compressor control. However, it can be readily extended to equipment having multiple stages of compression and fan speeds following the approach utilized in this work.

Acknowledgement

This work was supported by the California Energy Commission (CEC) with additional cost-sharing provided by Honeywell, Inc and Field Diagnostic Services, Inc.

References

[1] H. Li, J.E. Braun, A methodology for diagnosing multiple-simultaneous faults in vapor compression air conditioners, International Journal of Heating, Ventilating, Air Conditioning and Refrigerating Research, in press.
[2] M.S. Breuker, J.E. Braun, Common faults and their impacts for rooftop air conditioners, International Journal of Heating, Ventilating, Air Conditioning and Refrigerating Research 4 (3) (1998) 303–318.
[3] H. Li, J.E. Braun, An improved method for fault detection and diagnosis applied to packaged air conditioners, ASHRAE Transactions 109 (part 2) (2003) (Paper No. KC-03-8-2).
[4] T.M. Rossi, J.E. Braun, A statistical, rule-based fault detection and diagnostic method for vapor compression air conditioners, International Journal of Heating, Ventilating, Air Conditioning and Refrigerating Research 3 (1) (1997) 19–37.
[5] M.S. Breuker, J.E. Braun, Evaluating the performance of a fault detection and diagnostic system for vapor compression equipment, International Journal of Heating, Ventilating, Air Conditioning and Refrigerating Research 4 (4) (1998) 401–423.
[6] Bin Chen, J.E. Braun, Simple rule-based methods for fault detection and diagnostics applied to packaged air conditioners, ASHRAE Transactions 107 (part 1) (2001) (Paper No. AT-01-14-2, 847-837).
[7] Coby Davis, Comparison of steady state detection algorithms. ME 397 Report, Available from: Professor Jim Braun, Herrick Labs, Purdue University, West Lafayette, IN, USA, 1993.
[8] M.S. Breuker, Evaluation of a statistical, rule-based detection an diagnosis method for vapor compression air conditioners, Master's thesis, School of Mechanical Engineering, Purdue University, West Lafayette, IN, USA, 1997.
[9] T.M. Harms, Charge inventory system modeling and validation for unitary air conditioners, PhD thesis, School of Mechanical Engineering, Purdue University, West Lafayette, IN, USA, 2002.
[10] B. Shen, Experimental data for three R410a unitary air conditioners, Available from: Professor Jim Braun, Herrick Labs, Purdue University, West Lafayette, IN, USA, 2004.
[11] H. Li, A decoupling-based unified fault detection and diagnosis approach for packaged air conditioners, PhD thesis, School of Mechanical Engineering, Purdue University, West Lafayette, IN, USA, 2004.
[12] H. Li, J.E. Braun, Modeling adjustable throat-area expansion valves, in: Proceedings of the Tenth International Refrigeration and Air Conditioning Conference, Purdue University, West Lafayette, IN, USA, 2004 (Paper No. R130).
[13] H. Li, Experimental data for automated fault detection and diagnosis development, Available from: Professor Jim Braun, Herrick Labs, Purdue University, West Lafayette, IN, USA, 2005.
[14] T.M. Rossi, Detection, diagnosis, and evaluation of faults in vapor compression cycle equipment, PhD thesis, School of

Mechanical Engineering, Purdue University, West Lafayette, IN, USA, 1995.

[15] H. Li, J.E. Braun, On-line models for use in automated fault detection and diagnosis for HVAC&R equipment, in: Proceedings of the 2002 ACEEE Conference on Energy Efficiency in Buildings, Monterey, CA, USA, 2002.

[16] W.F. Stoecker, J.W. Jones, Refrigeration & Air Conditioning, second ed. McGraw-Hill, Inc., 1982.

[17] L. Yang, J.E. Braun, E.A. Groll, The impact of fouling on the performance of filter-evaporator combinations, in: Proceedings of the Tenth International Refrigeration and Air Conditioning Conference, Purdue University, 2004 (Paper No. R133).

[18] L. Yang, J.E. Braun, E.A. Groll, The impact of evaporator fouling on the performance of packaged air conditioners, in: Proceedings of the Tenth International Refrigeration and Air Conditioning Conference, Purdue University, 2004 (Paper No. R134).

[19] M.J. Brandemuehl, Algorithms and Subroutines for Secondary HVAC system Energy Calculations, Atlanta, American Society of Heating, Refrigerating, and Air-Conditioning Engineers, Inc., Atlanta, GA 30329, 1993.

[20] H. Li, J.E. Braun, Development of a virtual refrigerant charge level gauge, International Journal of Refrigeration, in preparation.

[21] B.N. Taylor, C.E. Kuyatt, Guidelines for evaluating and expressing the uncertainty of NIST measurement results, National Institute of Standards and Technology Technical Note 1297, U.S. Government Printing Office, Washington, DC 20402, 1994.

[22] ANSI/ARI Standard 540-1999, Positive Displacement Refrigerant Compressors and Compressor Units, American National Standards Institute, New York, NY 10036/Air-Conditioning and Refrigeration Institute, Atlanta, GA 30329, 2003.

[23] H. Li, J.E. Braun, Evaluation of a decoupling-based fault detection and diagnostic technique, International Journal of Heating, Ventilating, Air Conditioning and Refrigerating Research, in preparation.